JOURNAL OF APPLIED ELECTROCHEMISTRY 21 (1991) 301–307

Polymer electrolyte lithium batteries rechargeability and positive electrode degradation: an AC impedance study

R. KOKSBANG*, I. I. OLSEN, P. E. TONDER, N. KNUDSEN

Innovision A/S, Energy Research Laboratory, Hestehaven 21, DK-5260 Odense S, Denmark

D. FAUTEUX

Mead, Advanced Concepts Team, 3020 Newmark Drive, Miamisburg, Ohio 45342, USA

Received 29 May 1990; revised 14 August 1990

AC impedance measurements of polymer electrolyte-based, symmetrical composite cathode cells were used to probe the effects of the composite cathode composition and fabrication process upon its performance when used in polymer electrolyte-based thin film rechargeable lithium batteries. The relationship between cycling performance and AC impedance measurements were used to elucidate some of the reported failure mechanisms of rechargeable lithium polymer electrolyte batteries. The rapid initial capacity decay observed within the first few cycles of the polymer electrolyte/V_6O_{13} based composite cathode is shown to be related to the properties of the composite cathode active material, while the slower capacity decay observed during subsequent cycles, under continuous cycling regimes, appears to be related to a loss of ionic and electronic contact in the composite cathode.

1. Introduction

In 1978, Armand introduced the concept of solid organic polymers as solvents for electrolytes containing alkali metal salts [1, 2]. Following this discovery, the development of rechargeable all-solid-state lithium batteries based on solid polymer electrolytes and solid composite cathodes containing transition metal oxides and sulfides, have been an ongoing activity especially in the Mead/ERL joint venture [3, 4], at Harwell (UK) [5] and at Elf/Hydro Quebec [6, 7]. Significant progress in the development of this battery concept has been achieved in recent years. Higher electrolyte conductivity at lower temperatures and up-scaling from small laboratory test cells, to cells of sizes comparable to commercially available batteries, have been realized.

A basic requirement for a meaningful electrochemical experiment is the proper assembly of test cells, and the establishment of a 'perfect' interface between electrolyte and electrodes. When all-solid components are used, the establishment of proper interface contacts is an issue of major concern. Even in battery systems employing plastic solid organic polymer electrolytes, problems associated with interface contact are encountered. In some cases, it has been reported that the capacity of polymer electrolyte cells is observed to be unexpectedly low in the first discharge followed by a capacity increase during the next few cycles. This behaviour has been ascribed to an initial poor interfacial contact between electrolyte and electrode(s) which gradually improves during cycling [8]. Similarly, it is frequently reported that varying impedances are observed from cell to cell [9] or improvements of the interfacial properties are observed during the first few cycles [10]. In other cases, contrary to the behaviour described above, a rapidly declining capacity is observed. Recently, an investigation of solid polymer electrolyte cells employing $Li_{1+x}V_3O_8$ as the positive electrode active material was published. The extensive capacity decline, which took place over a relatively small number of cycles was ascribed to contact losses between cell components [11] because the lithium insertion reaction in this material was previously shown to be highly reversible [12].

AC impedance is a sensitive probe for characterization of electrode/electrolyte interfacial properties, especially in cells in which a reference electrode is incorporated because it is then possible to probe both individual interface impedances as well as the bulk properties. The method is widely used for characterization of the lithium/electrolyte interface, both in liquid electrolytes [13–17] and in solid polymer electrolyte based cells [18–25], for characterization of the positive electrode interface [9, 26–31] and for the characterization of the charge transfer process of lithium insertion in V_6O_{13} single crystals [32].

In the present paper, we attempt to correlate AC impedance measurements and cycling properties of polymer electrolyte based cells. Emphasis is placed on the dependence of the cathode/electrolyte interfacial

* Author to whom correspondence should be addressed.

0021-891X/91 $03.00 + .12

properties on both materials and processing parameters related to manufacture of cell laminates.

2. Experimental details

A polymeric electrolyte, based on a polymer host network electrolyte (PHNE) was formed by radiation polymerization of a polyether. The electrolyte conductivity was obtained by dissolving an electrolyte salt such as $LiAsF_6$ (Lithco) or $LiCF_3SO_3$ (FC-124, 3M) in the plasticized PHNE. The conductivity of the PHNE exceeds 1 mS cm^{-1} at room temperature [3, 4]. The active cathode material was V_6O_{13} (manufactured in-house at ERL), to which Shawinigan black and PHNE were added in order to realize a solid composite cathode. Lithium foil from Lithco was used as received as the anode material. The theoretical capacity of the solid composite cathode for each cell was determined by chemical analysis for vanadium.

The cells used for these experiments all had an area of 16–20 cm^2 and a thickness ranging from 100 to 200 μm. The laminate and test cell configurations are shown in Fig. 1. The reference electrode was either a 2 mm^2 active area lithium or LiAl strip attached to a copper current collector extending from the edge of the sealing. The LiAl reference electrodes were formed electrochemically by repetitive pulse shorting (short for 15 s, pause for 20 s) an 8 μm thick aluminium strip with the lithium electrode until a stable voltage of $\sim$380 mV against lithium was reached [33].

The cells were cycled at room temperature between limits of 1.8 and 3.0 V (100% DOD) and a constant current of 10^{-4} A cm^{-2}. Following the constant current charge to 3.0 V the cells were subject to a one hour potentiostatic charge period in order to compensate for the *IR* drop. A full 100% utilization of the material corresponds to insertion of 8 Li/V_6O_{13}.

The AC impedance measurements were conducted in the frequency range 65 kHz to 0.1 Hz, and occasionally to lower frequencies. The measurements were performed with a Solartron 1250 Frequency Responce Analyser connected to a Solartron 1286 Electrochemical interface used for polarizing the cells. The equipment was controlled by a personal computer which was also used for data collection and for least squares fitting [34]. All measurements on cycled cells were performed in the discharged state after $\sim$30 min equilibration at o.c.v. in order to eliminate polarization effects.

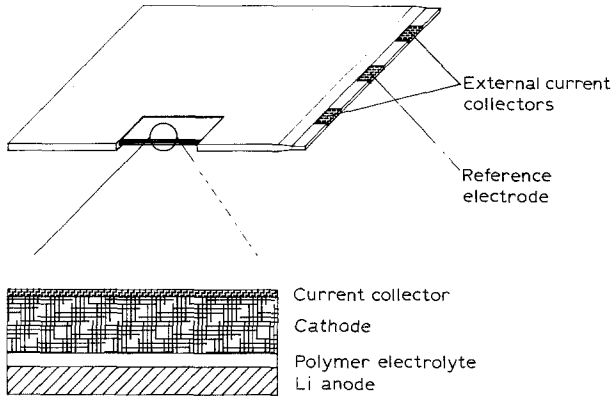

Fig. 1. Laminate and cell configuration.

All handling of materials and assembling of cells took place in either a dry room (< 2% r.h.) or in a glove box with a humidity and oxygen level lower than 10 ppm. The water contents of all starting materials were lower than 100 ppm as determined by Karl-Fischer titration.

3. Results and discussion

In Fig. 2a, the electronic equivalent diagram describing the composite cathode, the cathode/PHNE interfaces and composite cathode/current collector interface is depicted. In this model R_e denotes the resistance associated with the ionic conductivity of the bulk electrolyte. R_e is observed as an offset of the first semi-circle from the origin of the coordinate system. Z_i (R_i, C_i) represents the physical surface area of contact between the V_6O_{13} grains and the PHNE constituent of the composite cathode. Z_{ct} is the charge transfer impedance of lithium insertion in V_6O_{13}, W is the Warburg impedance related to the diffusion of Li^+

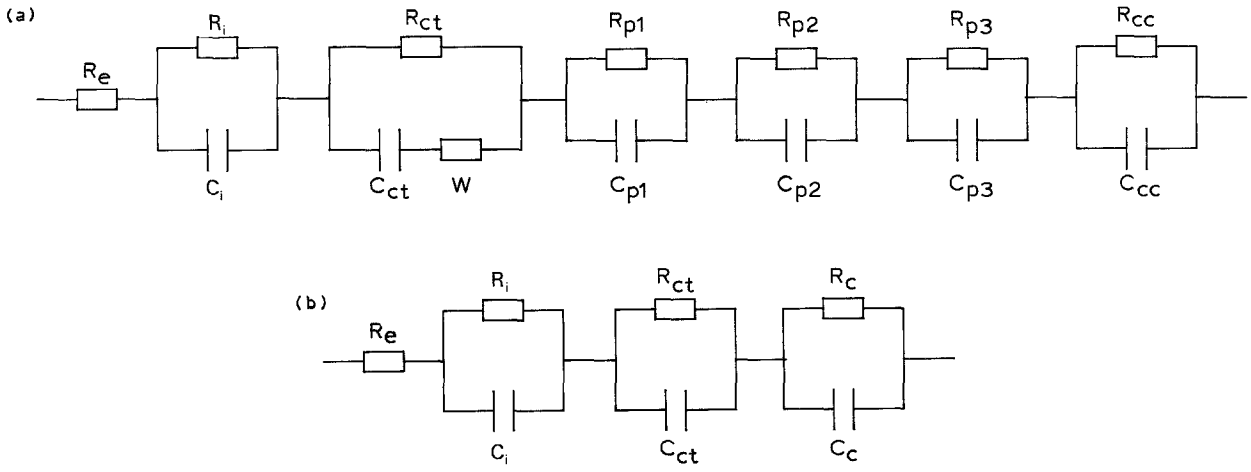

Fig. 2. Electronic equivalent circuit accounting for the electric properties of the composite cathode.

in the bulk V_6O_{13} grains, Z_{px} (x = 1, 2, 3) is the impedances associated with interparticle contact (V_6O_{13}–V_6O_{13}, V_6O_{13}–carbon and carbon–carbon) and Z_{cc} is related to the composite cathode/current collector contact and the geometric surface area of contact between the composite cathode and the PHNE separating the electrodes.

The interparticle contributions (V_6O_{13}–V_6O_{13}, V_6O_{13}–carbon, carbon–carbon) are impossible to distinguish from each other and from the composite cathode/current collector contribution under the experimental conditions applied in this work. The part of the equivalent circuit corresponding to these contributions to the impedance are therefore reduced to a simple parallel connection denoted R_c and C_c. Furthermore, the lithium ion diffusion in V_6O_{13} is neglected because its contribution to the impedance only occurs at lower frequencies. The electronic equivalent circuit diagram is, therefore, reduced to that shown in Fig. 2b.

In this diagram, the charge transfer resistance will contribute with a small fraction of the total impedance because of the high exchange current density associated with the lithium insertion reaction in V_6O_{13} ($\sim 3 \times 10^{-4}$ A cm^{-2} as calculated from single crystal data [32]) and the large surface area of contact between PHNE and V_6O_{13}. Thus, the major contributors to the cell impedance are basically related to interfacial contact properties of materials and components while the materials properties tend to be of minor importance.

3.1. *Symmetrical cathode/PHNE/cathode cells*

An AC spectrum of a symmetrical cathode/PHNE/cathode cell is shown in Fig. 3. Three semi-circles, with relaxation times corresponding to approximately 10^{-6} s (1), 10^{-4} s (2) and 10^{-2} s (3) can be resolved as indicated in the figure. The low frequency spur is caused by ion depletion of the electrolyte and will be neglected in the following. The temperature dependence of the semi-circles, as well as the dependence on

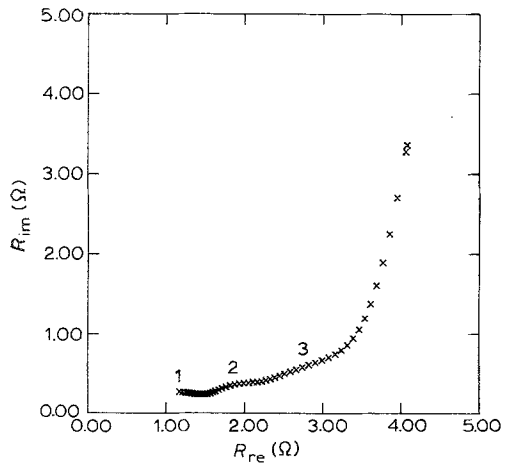

Fig. 3. Complex plane AC impedance diagram of symmetrical composite cathode/PHNE/composite cathode cell at room temperature. The fitting parameters associated with the corresponding equivalent circuit in Fig. 3b, are: R_i = 0.51 Ω, C_i = 4.2 × 10^{-6} F, R_{ct} = 0.67 Ω, C_{ct} = 2.2 × 10^{-4} F, R_c = 1.1 Ω, C_c = 6.1 × 10^{-3} F.

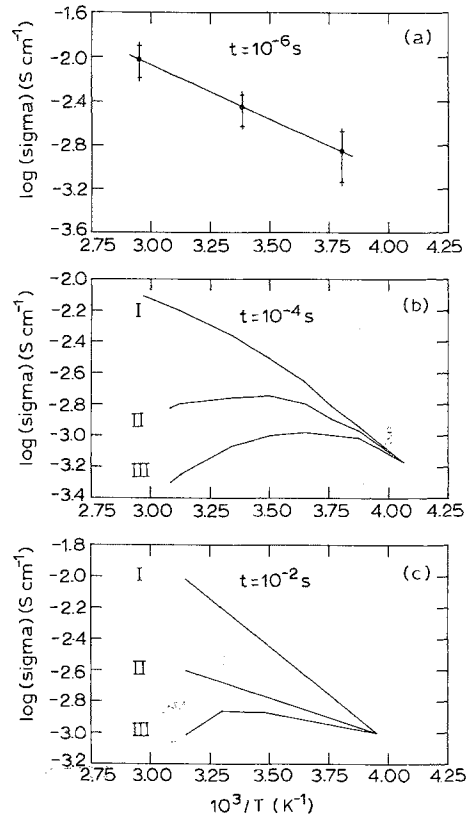

Fig. 4. Impedance variation vs temperature and process parameters of (a) semi-circle (#1), (b) semi-circle (#2) and (c) semi-circle (#3) as indicated in Fig. 3.

process parameters such as cathode composition and mixing, coating and lamination has been examined and is interpreted in the following where it should be noted that the semi-circle impedances are converted to equivalent conductivities.

Semi-circle (#1): The semi-circle associated with a relaxation time of 10^{-6} s (Fig. 4a) appeared to be strongly dependent on the V_6O_{13} content in the cathode. In cells without V_6O_{13} in the cathode, i.e. only PHNE and carbon present, this semi-circle is absent. Separation of the semi-circle from the larger semi-circle associated with a relaxation time of $\sim 10^{-4}$ s, appears at a V_6O_{13} content of $\sim$35 w/o. Increasing both V_6O_{13} and carbon content above this amount, has little or no effect on the magnitude of semi-circle #1. This semi-circle is therefore assigned to reactions which involve V_6O_{13}. The associated activation energy is 0.19 eV (±0.08 eV), i.e. considerably lower than that of the surface film on the anode ($\sim$0.6 eV [3]).

Semi-circle (#2): The temperature dependence of the semi-circle associated with a relaxation time of 10^{-4} s shows a less regular variation (Fig. 4b). However, a definite dependence on the total loading of the cathode with solid material (carbon and V_6O_{13}) was observed. A high weight fraction of solids in the cathode is related to high conductivity and an almost linear temperature dependence (curve I). At medium (curve II) and low (curve III) weight fractions of solid materials, an optimum conductivity is observed around room temperature. At low temperature the

three lines converge towards the high load line. As the behaviour is associated with the amount of carbon and V_6O_{13} present in the cathode, this semi-circle has been ascribed to interparticle contact, i.e. carbon–carbon, carbon–V_6O_{13} and V_6O_{13}–V_6O_{13} grain contacts. Consequently, this semi-circle will also be dependent on particle sizes and on process parameters associated with coating and mixing of the cathode materials as these steps are determining the properties of both the bulk cathode and the cathode/PHNE interface.

Semi-circle (#3): The conductivity related to this semi-circle associated with the 10^{-2} s relaxation time (Fig. 4c), shows a temperature dependence similar to that of semi-circle (#2). It was furthermore identified as depending on the lamination processes used and seems therefore to be related to the composite cathode/PHNE interface, i.e. the contact quality of the geometrical surface area between the two components. Furthermore, the magnitude of semi-circle #2 decreased when the adhesion between the composite cathode and the current collector was improved.

The studies of the impedance relations of the cathode/PHNE interface provide a tool for optimization of cathode performance with respect to interface quality (coating quality), solid loading vs impedance which is equivalent to an energy vs power relation, mixing quality of the cathode raw materials, particle size and cathode homogeneity and the quality of cathode formation (interparticle contact and particle-PHNE contact). Thus these measurements have been used to optimize cathode formulations, coatings, lamination and laminate configurations in order to achieve a satisfactory and reproducible battery performance. During optimization of cells with regard to the above mentioned materials and process parameters, AC impedance diagrams showing between one and three semi-circles were obtained (Fig. 3 and Figs. 6, 8, 9 upper traces).

3.2. *Impedance variation during cycling*

Results for three cells, identical in capacity, components thickness etc., with different cycling performance, are presented. All three cells show 100% utilization (8 Li/V_6O_{13}) in the first discharge. Also, impedances of cathode/PHNE interfaces and of the complete cells, are fairly identical before the first discharge, and corresponds to good lamination and interparticle contact.

As seen in Fig. 5, fast deterioration of the rechargeability is observed for the first cell. The poor rechargeability appears to be correlated with the development of the cathode/PHNE interface impedance (Z_{ca}) (Fig. 6). Initially only a single semi-circle and a low frequency spur are observed. The development of the shape of the semi-circle is generally towards higher interface impedance and a tendency of resolution of the single semi-circle present initially, in three semi-circles. The relaxation times of these semi-circles corresponds roughly to those of the three semi-circles

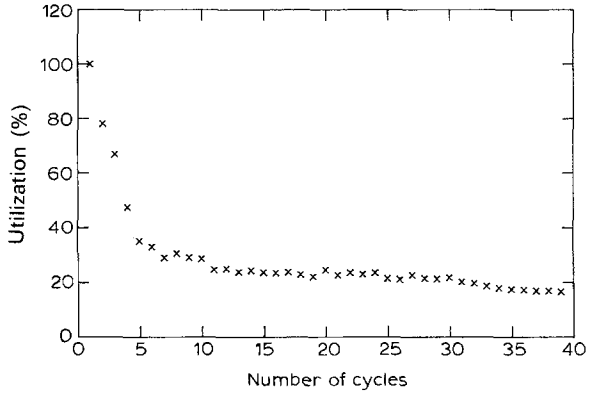

Fig. 5. Variation of the utilization of V_6O_{13} as function of number of cycles for a cell showing poor cyclability.

observed by measurements on symmetrical cathode/PHNE/cathode cells. In this case, semi-circles #2 and #3 are increasing appreciably in magnitude while the increase of semi-circle #1 is less pronounced. At cycle #24 all three semi-circles are resolved, implying that the electrode deterioration involves loss of contact between V_6O_{13} particles and PHNE in the solid composite cathode structure and either between the composite cathode and the current collector or the solid composite cathode and PHNE interfaces. The contact loss between the V_6O_{13} grains and the electrolyte constituent of the composite cathode is presumably related to the volume changes of V_6O_{13} which take place during lithium insertion and extraction ($\sim 10\%$ expansion by insertion of 8 Li/V_6O_{13} [35]) or to fragmentation of the V_6O_{13} particles. The latter results in isolated particles, inaccessible for further reaction.

In Fig. 7, the cycling performance of an initially well behaved cell is shown. Around cycle #20 the rechargeability performance suddenly deteriorates. The correlation between rechargeability and cathode/PHNE interface impedance is demonstrated by comparison with Fig. 8. Only one semi-circle and a low frequency spur is observed initially. After a few cycles a semi-circle with a relaxation time of 10^{-6} s is resolved implying that the interface properties between electrolyte constituent in the composite cathode and V_6O_{13} deteriorate. This semi-circle continues to grow

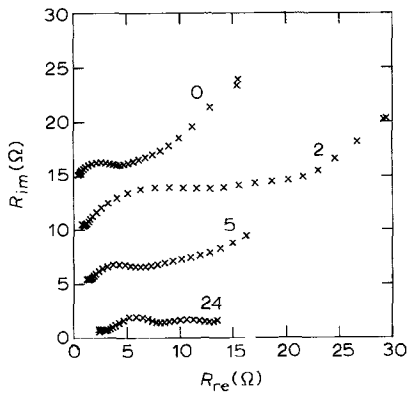

Fig. 6. Complex plane AC impedance diagrams in the discharged state (cathode only) as function of cycle number (indicated in the figure). See cycling performance in Fig. 5.

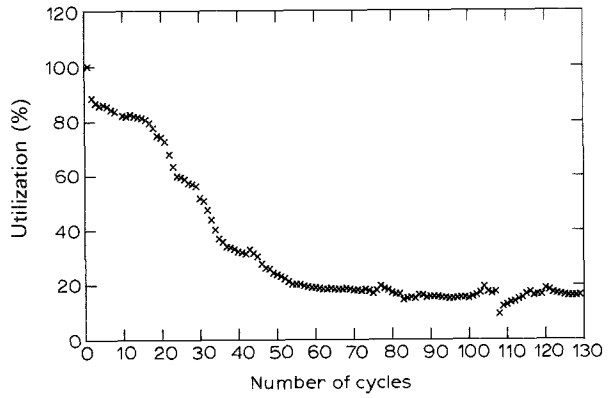

Fig. 7. Variation of V_6O_{13} utilization as function of number of cycles for an initially well behaving cell.

during continued cycling until cycle #17 whereafter it remains fairly constant. At cycle #17 the second semi-circle, at 10^{-4} s, starts to increase in magnitude and at higher cycle numbers and third semi-circle, at 10^{-2} s, also grows. The rechargeability deterioration observed from cycle #20 onwards, therefore, seems to be related to the two latter semi-circles, i.e. the deteriorating rechargeability properties are mainly related to loss of contact as was the case with cell #1.

The development of the cathode/PHNE interface impedance (Z_{ca}) of a battery performing as shown in Fig. 10c, is shown in Fig. 9. As in the two former cases, only one semi-circle and a low frequency spur are observed initially but only minor changes in the shapes of the curves are observed during cycling of the cell. Apart from the appearance of the small high frequency semi-circle, only a general increase in the magnitude of the interface impedance is observed but the gross features remain intact, consistent with the good rechargeability properties.

Another characteristic of the impedance measurements of all three cells, is the shift of R_e towards higher values. As the electrolyte conductivity as measured on

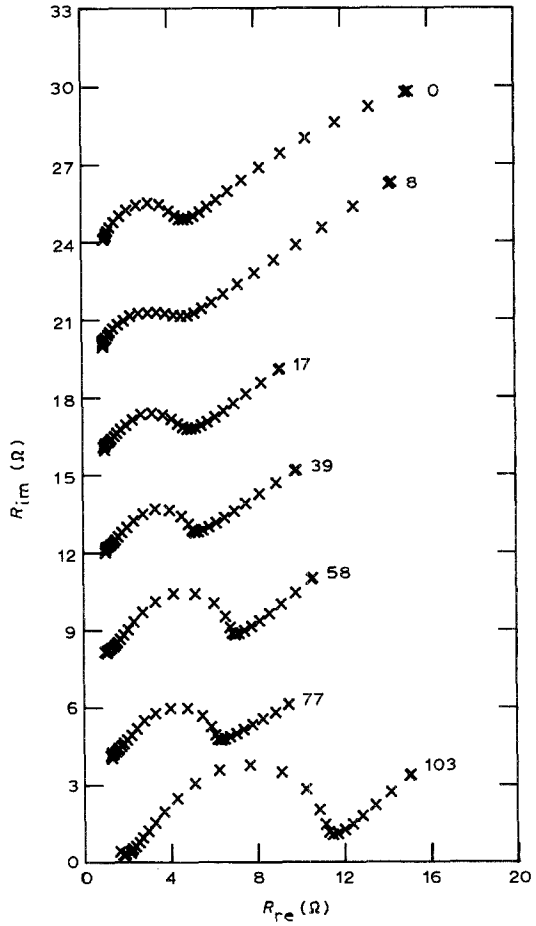

Fig. 9. Complex plane AC impedance plots in the discharged state (cathode only) as function of cycle number (indicated in the figure). See cycling performance in Fig. 10c.

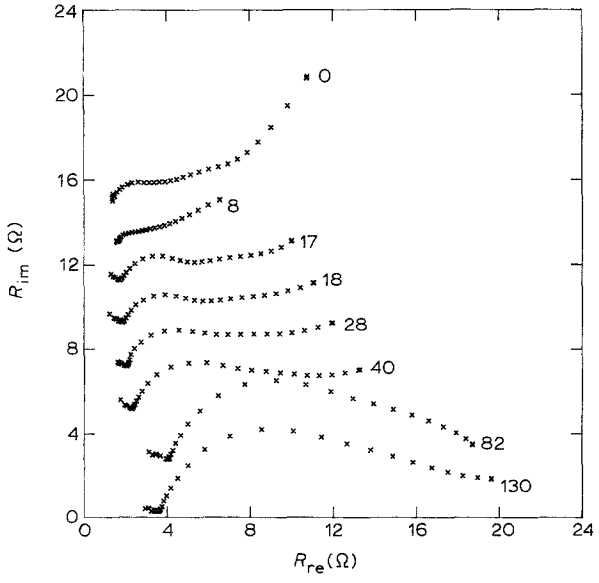

Fig. 8. Complex plane AC impedance plots in the discharged state (cathode only) as function of cycle number (indicated in the figure). See cycling performance in Fig. 7.

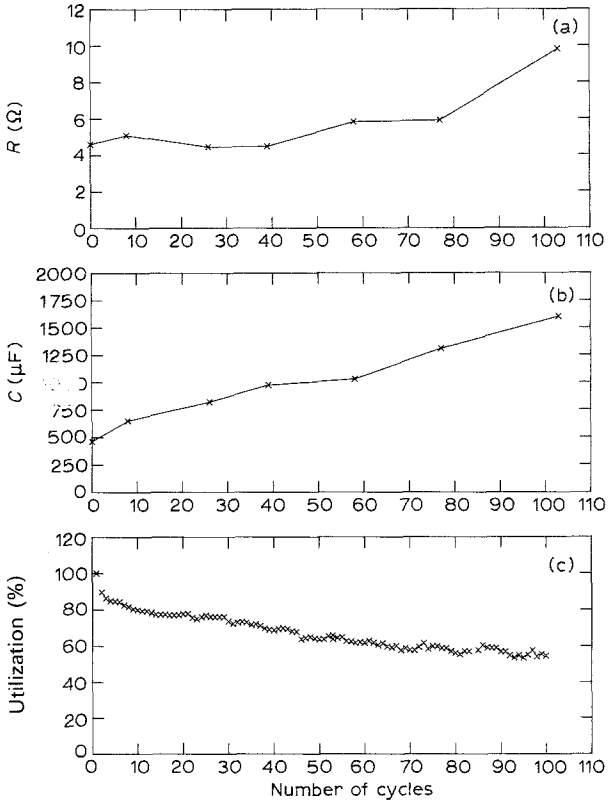

Fig. 10. (a) Interface resistance variation, (b) interface capacitance variation and (c) variation of V_6O_{13} utilization of V_6O_{13} as function of number of cycles.

metal/PHNE/metal (metal is Li and/or Ni) is time invariant, this phenomenon is also believed to be related to loss of contact.

In general, no severe changes are observed in the anode/PHNE interface impedance simultaneously with the occurrence of cell degradation. The properties of the composite cathode and the associated interfaces therefore seems to be responsible for cell failure. Furthermore, comparison of these results with the impedance measurements on symmetrical cathode/PHNE/cathode cells, permit a qualitative assessment of the reasons for cell failure. It appears that although the lithium insertion properties of V_6O_{13} degrade during cycling, the corresponding impedance contribution to the cell impedance is negligible. The poor cycling properties seems rather to be related to changes in the contact area, especially between the composite cathode and the current collector and between the V_6O_{13} and the PHNE constituent of the composite cathode.

The development of the capacity of the well performing cell (Fig. 10c) show an initial fast capacity decay ($\sim 10\%$ within the first ten cycles) followed by a slower, almost linear, capacity decay, reaching a loss of $\sim 40\%$ after 100 cycles. In an attempt to explain this behaviour a more detailed analysis of the corresponding impedance data was undertaken.

A simple impedance model was used for the interpretation of the high frequency properties of the impedance (Fig. 11). This model only takes into account the PHNE resistance (R_e) and the total cathode/PHNE interface resistance (R_i) and capacitance (C_i), and neglects effects related to diffusion etc. which are apparent at lower frequencies and the appearance of the small high frequency semi-circle (10^{-6} s) as this contribution to the total interface impedance is insignificant. Also the origin (chemical reaction, delamination, etc.) of the semi-circle is neglected as the model is only used for the case in which the three semi-circles are difficult or impossible to distinguish from each other. The development of R_i and C_i during cycling are shown in Figs 10b and 10c.

These measurements indicate that the initial steep capacity decline ($\sim 1\%$ per cycle) is related to changes in the composite cathode structure. This is only reflected in minor changes in the cathode/PHNE interface resistance, R_{ca}, as well as in the corresponding capacitance, C_{ca}, which is increasing almost linearly, reaching a value three times higher than the initial value after 100 cycles. The relaxation time, $t_{ca} = R_{ca}C_{ca}$ increase as a function of the cycle number, confirming that contact area properties are the major contributor to the impedance.

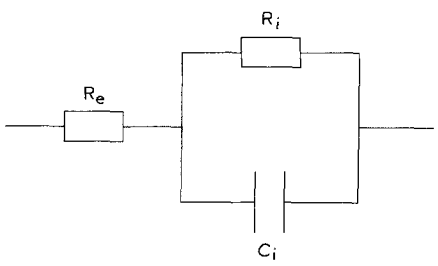

Fig. 11. Reduced equivalent circuit used for data fitting of the impedance data shown in Fig. 9. R_e is the resistance contribution from the bulk electrolyte and R_i, C_i are representing the combined interface impedances.

The origin and nature of the changes are not firmly established, but are presumably related to the volume changes which V_6O_{13} undergoes during cycling. On prolonged cycling a far less steep decline ($\sim 0.3\%$ per cycle) continues to diminish the available capacity. The *IR* drop, calculated from the total cell impedance (electrolyte resistance and interface impedances) measured under o.c.v. conditions, is less than 0.1 V after 100 cycles, i.e. far too low to account for the observed capacity decline ($\sim 40\%$). This behaviour is therefore apparently relatively independent of the interface impedances provided these are optimal initially. The low frequency spur, neglected so far, also seems to change during cycling and it is therefore possible that the charge retention is related to degrading diffusion properties of the composite cathode. This is furthermore supported by the fact that full utilization of the active material is recovered by decreasing the discharge current by a factor of ten. However, the present data are insufficient for a detailed analysis at lower frequencies.

4. Conclusion

The AC impedance measurements on symmetrical cathode/PHNE/cathode cells have shown that the magnitude and nature of the interface impedances are strongly dependent on the processing of the composite cathode materials, i.e. mixing, coating and lamination as well as on both the total amount of solids and the amount of V_6O_{13} present in the cathodes.

Proper mixing of the raw materials and coating of the cathode paste/slurry reduce the impedance as do high amounts of solids, the latter indicating that the impedance of the 'bulk' cathode is primarily determined by the electronic conductivity rather than the ionic conductivity.

When the V_6O_{13} content exceeds 35 w/o, a high frequency semi-circle is resolved. The magnitude of the semi-circle appears to be independent of the V_6O_{13} content above 35 w/o and is either associated with the lithium ion insertion in V_6O_{13} as such or as with the formation of a cathode/PHNE interface layer [28–30] due to reaction between V_6O_{13} and the polymer electrolyte constituents of the composite cathode. However, during this study, no strong evidence was found for formation of an interface layer.

The largest contribution to the cathode/PHNE interface impedance is related to lamination of the composite cathode and the PHNE separator and adhesion of the composite cathode to the current collector. These contributions cannot be distinguished from each other, but improved adhesion of the composite cathode to the metal foil current collector, reduced the impedance significantly.

These results were used to interpret impedance data obtained during cycling of complete cells equipped with reference electrodes. Results for three identical cells with similar impedance characteristics and cycled under identical conditions, are compared. Full utilization of the active material, corresponding to 8 Li/V_6O_{13}, was achieved during first discharge of all three cells. However, during continued cycling the capacity retention developed differently. A correlation between the cycling performance and the cathode/PHNE interface impedance is evident. In the worst case, a rapidly deteriorating capacity is mirrored in transformation of the single semi-circle present initially, into three semi-circles after a few cycles. This behaviour is interpreted as delamination of the cathode components, i.e. loss of contact between cathode and current collector and/or PHNE separator. Furthermore, loss of interparticle contact and loss of contact between the V_6O_{13} grains and the PHNE constituent was observed.

In the best case, the initial fast capacity decay (10–15% within $\sim$10–15 cycles) appeared to be related to the composite cathode. Only minor changes of the cathode/PHNE interface impedance and the corresponding capacitance was observed. During extended cycling, the slower capacity decay appeared to be related to a loss of ionic and electronic contact in the composite cathode. The results demonstrate that the impedance variations can be explained solely by contact area considerations without taking into account, for example, film formation on the electrolyte/V_6O_{13} interface due to reaction between cathode and electrolyte constituents, as suggested by Bruce *et al.* [28–30].

Acknowledgements

The authors appreciate the many fruitful discussions with Dr S. Yde-Andersen, ERL, and Dr E. Skou, University of Odense.

References

[1] M. B. Armand, J. M. Gabano and M. Duclot, Second International Meeting on Solid Electrolytes, St. Andrews, Scotland, 20–22 September 1978, Extended abstract no. 6.5.

[2] *Idem*, in 'Fast Ion Transport in Solids. Electrodes and Electrolytes', (edited by P. Vashishta, J. N. Mundy, G. K. Shenoy), North-Holland, New York (1979) pp. 131–136.

[3] J. S. Lundsgaard, S. Yde-Andersen, R. Koksbang, D. R. Shackle, R. A. Austin and D. Fauteux in Proceedings of the Second International Symposium on Polymer Electrolytes (edited by B. Scrosati), Siena, Italy, 14–16 June 1989, Elsevier, London (1990) pp. 395–410.

[4] R. Koksbang, I. I. Olsen, P. E. Tonder, N. Knudsen, J. S. Lundsgaard and S. Yde-Andersen, *J. Power Sources* **32** (1990) 175.

[5] A. Hooper and J. Jensen (eds), 'Advanced Battery Development. Solid State Rechargeable Lithium Batteries – Anglo/Danish Project Phase II', Final Summary Report for the period 1st September 1980–31st March 1984, EEC Energy Conservation programme, Odense University Press, Denmark (1984).

[6] M. Gauthier, D. Fauteux, G. Vassort, A. Belanger, M. Duval, P. Ricoux, J. M. Gabano, D. Muller, P. Ricaud, M. B. Armand and D. Deroo, *J. Electrochem. Soc.* **132** (1985) 1333.

[7] M. Gauthier, A. Belanger, B. Kapfer, G. Vassort and M. Armand in 'Polymer Electrolyte Reviews 2', (edited by J. R. MacCallum and C. A. Vincent, Elsevier Applied Science, London) (1989) pp. 285–332.

[8] S. Skaarup, K. West, B. Zachau-Christiansen and T. Jacobsen in 'Proceedings of the International Seminar on Solid State Ionic Devices', (edited by B. V. R. Chowdari and S. Radhakrishna), World Scientific Publishing, Singapore (1988) pp. 75–86.

[9] C. C. Hunter, D. C. Sinclair, A. R. West and A. Hooper, *J. Power Sources* **24** (1988) 157.

[10] B. Scrosati, *J. Electrochem. Soc.* **136** (1989) 2774.

[11] *Idem, Brit. Polym. J.* **20** (1988) 219.

[12] S. Panero, M. Pasquali, M. Tocci and G. Pistoia, *J. Electrochem. Soc.* **130** (1983) 1225.

[13] J. Thevenin, *J. Power Sources* **14** (1985) 45.

[14] J. G. Thevenin and R. H. Muller, *J. Electrochem. Soc.* **134** (1987) 273.

[15] D. H. Shen, S. Subbarao, F. Deligiannis and G. Halpert in 'Proceedings of the Symposium on Materials and Processes for Lithium Batteries', (edited by K. M. Abraham, B. B. Owens), The Electrochemical Society, 89–4, Pennington NJ (1989) pp. 223–36.

[16] R. V. Moshtev and B. Puresheva, *J. Electroanal. Chem.* **180** (1984) 609.

[17] G. Montesperelli, P. Nunziante, M. Pasquali and G. Pistoia, *Solid State Ionics* **37** (1990) 149.

[18] F. Bonino, B. Scrosati, A. Selvaggi, J. Evans and C. A. Vincent, *J. Power Sources* **18** (1986) 75.

[19] M. Hiratani, K. Miyauchi and T. Kudo, *Solid State Ionics* **28–30** (1988) 1431.

[20] P. W. M. Jacobs, J. W. Lorimer, A. Russer and M. Wasiucionek, *J. Power Sources* **26** (1989) 483.

[21] P. Ravn Sorensen and T. Jacobsen, *Electrochim. Acta* **27** (1982) 1671.

[22] S. Morzilli, F. Bonino and B. Scrosati, *ibid.* **32** (1987) 961.

[23] F. Croce, R. Curini, S. Pentaloni, S. Passerini, A. Selvaggi and B. Scrosati, *J. Appl. Electrochem.* **18** (1988) 401.

[24] D. Fauteux, *Solid State Ionics* **17** (1985) 133.

[25] *Idem, J. Electrochem. Soc.* **135** (1988) 2231.

[26] B. C. H. Steele, G. E. Lagos, P. C. Spurdens, C. Forsyth and A. D. Foord, *Solid State Ionics* **9/10** (1983) 391.

[27] B. V. Ratnakumar, S. Di Stefano and C. P. Bankston, *J. Appl. Electrochem.* **19** (1989) 813.

[28] M. G. S. R. Thomas, P. G. Bruce and J. B. Goodenough, *J. Electrochem. Soc.* **132** (1985) 1521.

[29] P. G. Bruce and F. Krok, *Electrochim. Acta* **33** (1988) 1669.

[30] *Idem, Solid State Ionics* **36** (1989) 171.

[31] F. C. Laman, J. A. R. Stiles, R. J. Shank and K. Brandt, *J. Power Sources* **14** (1985) 201.

[32] T. Jacobsen, K. West, B. Zachau-Christiansen and S. Atlung, *Electrochim. Acta* **30** (1985) 1205.

[33] R. Koksbang, D. Fauteux, P. Norby and K. A. Nielsen, *J. Electrochem. Soc.* **136** (1989) 598.

[34] B. A. Boukamp, *Solid State Ionics* **11** (1984) 339.

[35] K. West, B. Zachau-Christiansen and T. Jacobsen, *Electrochim. Acta* **28** (1983) 1829.